Massive parallel laser shock peening: Simulation, analysis, and validation

A.W. Warren [a], Y.B. Guo [a,*], S.C. Chen [b]

[a] Department of Mechanical Engineering, The University of Alabama, Tuscaloosa, AL 35487, United States
[b] Department of Mechanical Engineering, The University of Texas at Austin, Austin, TX 78712, United States

Abstract

Laser shock peening (LSP) is a transient process with laser pulse duration time on the order of 10 ns, real time in situ measurement of laser/material interaction is very challenging. LSP is usually performed in a massively parallel mode to induce uniform compressive residual stress across the entire surface of the workpiece. The purpose of this paper is to investigate the effects of parallel multiple laser/material interactions on the stress/strain distributions during LSP of AISI 52100 steel.

FEA simulations of LSP in single and multiple passes were performed with the developed spatial and temporal shock pressure model via a subroutine. The simulated residual stresses agree with the measured data in nature and trend, while magnitude can be influenced by the interactions between neighboring peening zones and the locations of residual stress measurement. A design-of-experiment (DOE) based simulation of massive parallel LSP were also performed to determine the effects of laser intensity, laser spot size, and peening spacing on stresses and strains. Increasing the laser intensity increases both the stress magnitude and affected depth. The use of smaller laser spot sizes decreases the largest magnitude of residual stress and also decreases the depth affected by LSP. Larger spot sizes have less energy attenuation and cause more plastic deformation. Spacing between peening zones is critical for the uniformity of mechanical properties across the surface. The greatest uniformity and largest stress magnitudes are achieved by overlapping of the laser spots.
© 2007 Elsevier Ltd. All rights reserved.

Keywords: Laser shock peening; Laser/material interaction; FEA; Residual stress

1. Introduction

Laser shock peening (LSP) is a surface treatment process designed to improve the mechanical properties and fatigue performance of materials. LSP is primarily conducted on metallic components. The principle of LSP is to use a high intensity laser and suitable overlays to generate high pressure shock waves on the surface of the workpiece.

An increase in fatigue strength is accomplished by the creation of large magnitudes of compressive residual stresses and increased hardness which develop in the subsurface. The maximum compressive residual stress is often formed at the surface of the workpiece and decreases in magnitude with increasing depth below the surface. The transient shock waves can also induce microstructure changes near the surface and cause high density of dislocations to be formed. The combined effect of the microstructure changes and dislocation entanglement contribute to an increase in the mechanical properties in the near surface.

It has been shown by previous research [1–8] that improved fatigue life of metallic components such as bearings, gears, shafts, etc. can be accomplished by inducing compressive residual stress and work hardening in the subsurface. The compressive residual stresses also improve resistance to corrosion fatigue. An advantage of LSP is that the magnitude of affected depth is very deep as compared with other surface processes such as conventional shot peening. In the case of rolling contact such as bearings,

* Corresponding author. Tel.: +1 205 348 2615; fax: +1 205 348 6419.
E-mail address: yguo@eng.ua.edu (Y.B. Guo).

the residual impressions from the LSP can also improve fatigue life by acting as reservoirs for lubricant.

During LSP (Fig. 1), the surface of the test specimen is usually first coated with a thin layer of material such as black paint which is opaque to the laser beam. This opaque layer acts as sacrificial material and is converted to high pressure plasma as it absorbs energy from a high intensity laser (1–10 GW/cm^2) for very short time durations (<50 ns). If the specimen surface is also submerged in a transparent media such as water, the rapidly expanding plasma cannot escape and the resulting shock wave is transmitted into the specimen subsurface. These shock waves can be much larger than the dynamic yield strength of the material (>1 GPa) and cause plastic deformation to the surface and compressive residual stresses which can extend to a deep depth in the subsurface. Due to the high strains/strain rates that the material undergoes, there can also be significant microstructure changes thus causing the mechanical properties such as hardness, tensile strength, and fatigue strength to be improved. Because thermal rise in the specimen is nearly eliminated by the water overlay, LSP is a primarily a mechanical process. In order to make the improved material properties more uniform, massive LSP zones must be created. It may also be advantageous to perform multiple LSP passes in order to create larger magnitudes of residual stress and hardness.

Previous LSP simulations have focused on a single laser peened zone. While these simulations are valuable for obtaining insight of the physical process by which the shock wave is propagated through the specimen, they may not accurately reflect the real process of LSP. In actual applications, multiple locations of the workpiece are usually shock peened in a massive parallel mode to accomplish uniform surface properties across the entire specimen surface. Single LSP simulation is only applicable to cases where the spacing between consecutive peening zones is sufficiently large. If the LSP zones are denser, the interaction between consecutive peened zones will become a significant factor for estimation of LSP affected depth, residual stresses, surface properties, and surface profiles.
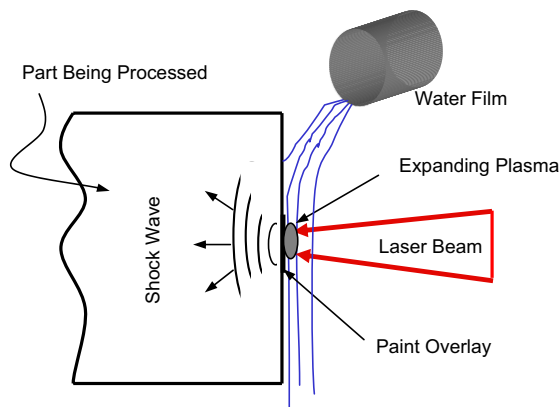
The objective of this research is to create a 3D finite element model to reveal the interactions between massive parallel laser shock peening of AISI 52100 steel. This will be accomplished in two steps. The first is to perform a simulation which can be compared to the experimental residual stress data [9]. A user subroutine has been created, for the first time, to model massive parallel laser shock pressure as a function of time and space. After this benchmark simulation was completed, a design-of-experiment (DOE) based sensitivity analysis was performed to test the effects of laser intensity, laser spot size, and peening spacing on stresses and strains.

This work sheds light on the complex interactions of massive parallel LSP to enable LSP process parameters to be properly selected to achieve optimal surface integrity. The effects of laser intensity, laser spot size, and peening spacing are critical to surface integrity characteristics such as residual stress, microstructure, and surface quality.

2. Literature review

A significant amount of LSP research has been conducted to investigate the surface integrity of metallic components. Most experimental work has focused on the determination of residual stress magnitudes and distributions at the surface and in-depth subsurface. The effect of LSP on mechanical properties such as hardness, fatigue strength, and fatigue life has been studied [10,11], however, more research is still needed. The resulting surface integrity can be correlated with the LSP process parameters such as laser intensity, laser spot size, peening pass, and peening spacing. The recent status of research and development on LSP of metals has been reviewed [12].

A primary goal of LSP is to induce deep compressive residual stress and work hardening in the surface of the workpiece. The depth and magnitude of compressive residual stress can vary depending on the LSP process parameters. Increasing the laser intensity increases both the magnitude and affected depth of the induced compressive stress in the subsurface. However, it has been shown that laser intensities greater than a particular threshold serve to decrease the surface stress magnitude, but continue to increase the magnitude and affected depth in the subsurface [3]. This was attributed to expansion release waves that are formed due to high energy shock waves. An investigation of laser spot size effect showed that energy attenuation is less for larger spot sizes allowing the stress shock wave to propagate deeper into the material [13]. Thus larger spot sizes increase the depth of plastic deformation. Laser peening across the entire specimen surface allows uniform mechanical properties. Peening spacing is critical to provide uniformity of mechanical properties across the entire surface. A study of overlapped laser spots [2,3,14,15] showed that the residual stress distribution is nearly uniform and is entirely compressive. Hardness decreases in the area between adjacent laser spots that do not overlap. When the spacing between adjacent peened zones is

Fig. 1. Schematic of laser shock peening (LSP).

increased, the mechanical properties can vary significantly across the surface.

Previous numerical simulations of LSP have been performed to gain better understanding of the physical process. Because LSP is a highly transient process, it is difficult (if not impossible) to experimentally observe and quantify the stress wave propagation into the specimen surface. Many researchers have used finite element simulations to gain insight into the process. Simulations have been used to aid in determining accurate shock pressure models, verify experimental data, and predict residual stress profiles. Zhang et al. [16] improved the shock pressure models of Clauer [17] and Fabbro [18] by accounting for the non-linear mass transfer of LSP. The model also accounts for the time dependent radial expansion of plasma for microsized laser peening. Finite element simulations have been performed to verify and predict the residual stress profiles after LSP [19–21]. Although these simulations have studied the effect of multiple laser passes, they have been limited to a single laser spot for both two- and three-dimensional modeling. A 3D massive parallel LSP simulation scheme is essential to improve fundamental understanding of LSP and the resultant surface integrity.

3. Numerical simulations

3.1. Simulation scheme

The benchmark simulation is to verify that the single and two passes of LSP simulation produced similar residual stress magnitudes and distributions as experimentally observed by Yakimets et al. [9]. The benchmark simulation consisted of a single laser peening located at the center of the workpiece as shown in Fig. 2. The simulation condition is also shown. The benchmark simulation mesh consisted of 95,000 C3D8R-type elements. Elements size was biased with a higher density of elements near the surface and gradually becoming less dense with increasing depth below the surface. The elements along the edges and bottom surface are semi-infinite elements to prevent reflective boundaries for the shock wave. The initial residual stress values in

the transverse, longitudinal, transverse shear, and longitudinal shear directions were input according to the experimental data [9] as −62 MPa, −152 MPa, −56 MPa, and −23 MPa, respectively.

The DOE based simulation is a sensitivity analysis to determine the effects of laser intensity, laser spot size, and peening spacing. The sensitivity analysis mesh consisted of 252,000 C3D8R-type elements as shown in Fig. 3. The sensitivity analysis was performed as a 3 × 3 matrix with laser intensity, laser spot size, and spacing shown in Table 1. An adaptive mesh was used for both cases to accommodate the large stress wave magnitudes that are associated with LSP. The workpiece material is AISI 52100 steel with properties shown in Table 2.

3.2. Spatial and temporal shock pressure modeling via a subroutine

A subroutine VDLOAD has been programmed to apply the non-uniform shock pressure. This subroutine allows the pressure intensity to vary simultaneously with respect to radial distance from the center of the laser spot and elapsed time of the laser pulse. It works by assigning local origins at the center of the desired shock peen locations and calculates the radial distance to each node surrounding this new origin from the equation of a circle as

$$r = \sqrt{(curcoords(i,1))^2 + (curcoords(i,2))^2} \tag{1}$$

where $curcoords(i,1)$ and $curcoords(i,2)$ are the coordinates in the 1 and 2 directions, respectively, for the current node at each time increment of the analysis.

The pressure as a function of radial distance from the center of the laser spot follows a Gaussian distribution. Maximum pressure is located at the center of the laser spot and decreases with increasing radial distance from the center.

The pressure distribution is also a function of the elapsed time of laser pulse. The pressure is initially zero and reaches a peak value when the elapsed time equals the total pulse time. Following the results by Zhang et al.

S, S33
(Ave. Crit.: 75%)
+1.074e+08
−1.947e+08
−4.968e+08
−7.989e+08
−1.101e+09
−1.403e+09
−1.705e+09
−2.007e+09
−2.309e+09
−2.611e+09
−2.914e+09
−3.216e+09
−3.518e+09

Simulation Parameters:
Laser intensity = 4 GW/cm^2
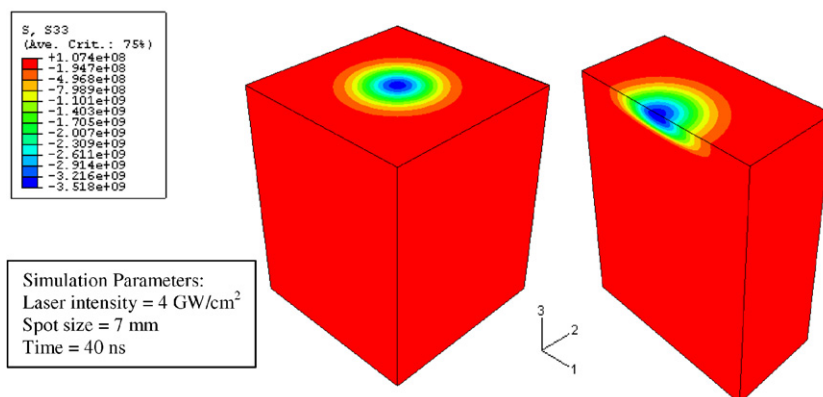Spot size = 7 mm
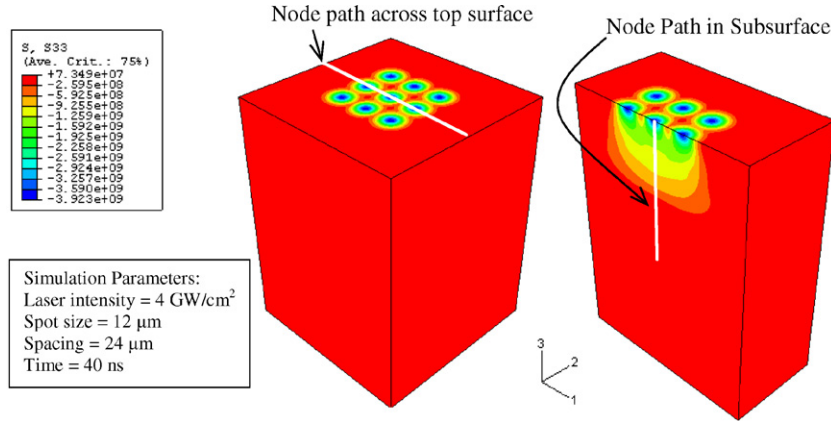Time = 40 ns

Fig. 2. Benchmark simulation model of single LSP.

Fig. 3. Simulation model of massive parallel LSP.

Table 1
Design of experiment based LSP sensitivity parameters

Simulation parameter	Value		
Intensity (GW/cm^2)	2	4	6
Laser radius R (µm)	3	6	12
Spacing (µm)	R	$2R$	$4R$

Table 2
Mechanical properties of AISI 52100 steel (62HRC)

Material property	Value
Density (kg/m^3)	7800
Poisson's ratio	0.27
Young's modulus (GPa)	209
Yield strength (MPa)	1650

[16], the pressure versus time relationships can be well represented as fourth-order polynomials to follow the pressure versus time relationships shown in Fig. 4.

The pressure $P(r,t)$ at any point and time can be calculated as

$$P(r,t) = P(t) \exp\left(-\frac{r^2}{2R^2(t)}\right) \tag{2}$$

where $P(t)$ is the pressure at time t during the laser pulse interpolated from Fig. 4, r is the radial distance from the center of the laser spot in Eq. (1), and $R(t)$ is the laser spot radius.
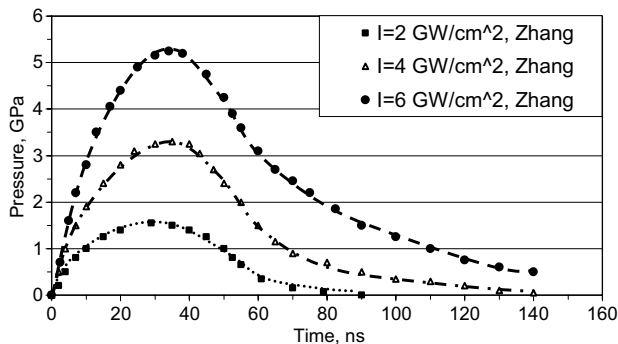
The very short pulse duration (40 ns) makes the simulation an ideal transient case. For this purpose, Abaqus/Explicit [22] was used to implement the simulation scheme. The benchmark simulation was performed as both a single and double pass of laser shock peening. The procedure involved applying a laser pulse for 40 ns then removing the load. The load was removed long enough for the stresses to stabilize and then reapplied for 40 ns and unloaded again. The results for single and double pass were taken at the end of the first and second unload sequences, respectively.

3.3. DOE based sensitivity simulation

As listed in Table 1, three levels of laser intensity, spot size, and spacing were used to conduct the sensitivity analysis. The laser shock pressure follows a model created by [16] which defines the pressure versus time as a function of laser intensity. For this analysis, three laser intensities were considered: 2 GW/cm^2, 4 GW/cm^2, and 6 GW/cm^2. The shock pressure versus time plot is shown in Fig. 4.

Laser spot size effect was evaluated by performing a series of simulations in which the laser radius was varied. The laser radii used were 3, 6, and 9 µm which correspond to spot sizes of 6, 12, and 24 µm, respectively.

The effect of peening spacing was studied by adjusting the distance between the centers of adjacent shock zones. Spacing for this analysis is defined as the distance between centers of adjacent laser shocked zones. The spacing used in this analysis is as follows: R, $2R$, and $4R$ where R is the radius of the laser spot. For example, a laser spot size of 12 µm would have a radius of 6 µm. The different spacing distances would then be 6, 12, and 24 µm. For the spacing $= R$ case, the laser spots would overlap 50%, while the spacing $= 2R$ would align the laser spots edge to edge. The spacing $= 4R$ allows enough distance that the laser spots do not overlap.

Fig. 4. Pressure versus time as a function of laser intensity.

4. Results and discussion

4.1. Benchmark simulation and verification

The predicted residual stresses were obtained from the surface element located at the center of the laser spot. A comparison of the measured and simulated residual stress values are shown in Figs. 5 and 6. Both the predicted and measured residual stresses are compressive, so they agree with the nature and trend. There is some discrepancy between the two which may be due to several factors that differentiate the experimental procedure from the simulation. In addition to numerical errors, the first is the massive parallel LSP used for the experiment which was not accounted for in the benchmark simulation. The overlaps of consecutive laser peenings that occurred in LSP experiments would increase the magnitudes of compressive residual stress. The predicted residual stresses from both single and two LSP passes are expected to be lower than those from the experiments. The second is that the X-ray diffraction technique using Cr K_α radiation actually measures an average residual stress in the depth of X-ray penetration (5–10 μm). In addition, the exact location of residual stress measurement with regard to the laser peened zone cannot be accurately controlled for the experiment. For the measurement itself, the residual stress magnitudes across the peened surface are different just due to the non-uniform nature of surface integrity. Unless high precision calibration and control can be carried out first, the X-ray and other non-destructive measurement methods are only useful for comparative purpose.

4.2. Design of experiment based sensitivity analysis

The stress and strain results for the sensitivity analysis were extracted from a node path that goes through the center of the laser spots across the top surface and a node path directly beneath the central laser spot as shown in Fig. 3.

4.2.1. Intensity effect

Stresses across top surface: The effect of intensity was plotted for a series of simulations which used a constant

Fig. 6. Comparison of predicted surface residual stress s22 with measured data.

spot size of 9 μm and peening spacing of 9 μm. For each case only the laser intensity was varied. Fig. 7a shows the influence of intensity on von Mises stress across the top surface. As intensity is increased from 2 GW/cm² to 4 GW/cm² the magnitude of von Mises stress is increased by over 300%, while increasing from 4 GW/cm² to 6 GW/cm² only increases the magnitude by 75%. A similar trend is seen in the surface stress s11 in Fig. 7b. Stress s22 is the same as s11 due to the symmetrical load and workpiece geometry and will not be reported. Fig. 7c shows the magnitude of the surface stress along the direction of shock wave propagation experienced at maximum pressure. Peak stress magnitudes are located at the center of each shock peened zone, however, the central spot is slightly higher due to the influence from the adjacent laser peened areas.

Strains across top surface: The magnitude of the normal strain le33 is substantially larger (10×) than the transverse strains le11 and le22. In order to make this paper concise, only le33 will be discussed. Fig. 7d shows the surface distribution of le33 for the varying laser intensities. Peak strains occur at the center of each laser spot with the maximum strain occurring at the central laser spot. This is due to the combined effect of the adjacent laser peened zones.

Stresses in subsurface: von Mises stress in the subsurface is shown in Fig. 7e. For $I = 2$ GW/cm², the maximum von Mises stress occurs at a depth of 4 μm. For 4 and 6 GW/cm² the von Mises stress plateaus at a value equal to the

Fig. 5. Comparison of predicted surface residual stress s11 with measured data.
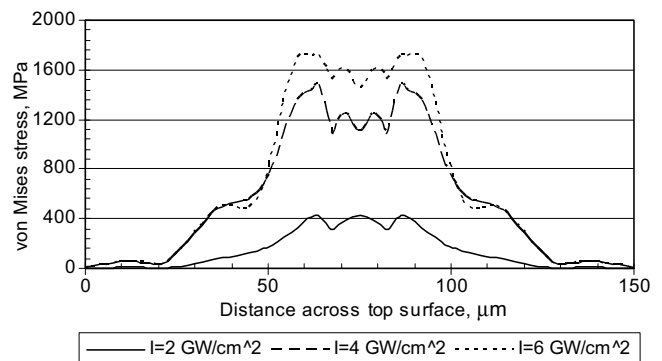
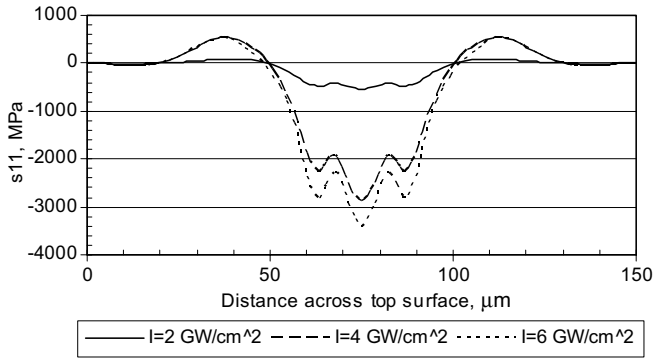Fig. 7a. Intensity effect on von Mises stress.
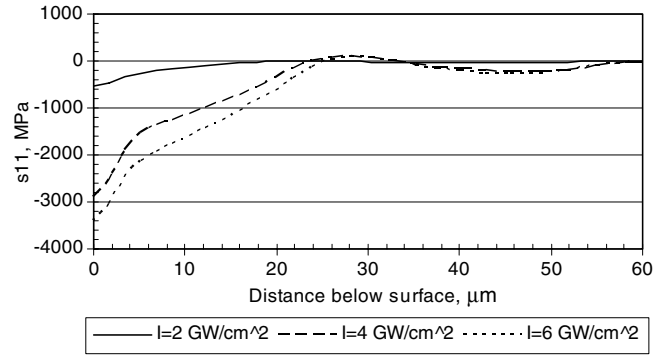
Fig. 7b. Intensity effect on s11.

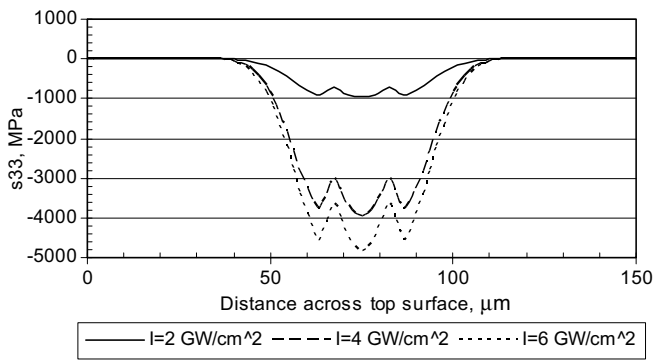Fig. 7f. Intensity effect on s11.

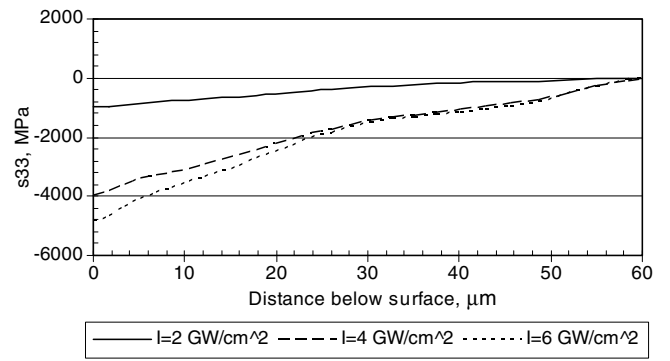Fig. 7c. Intensity effect on s33.
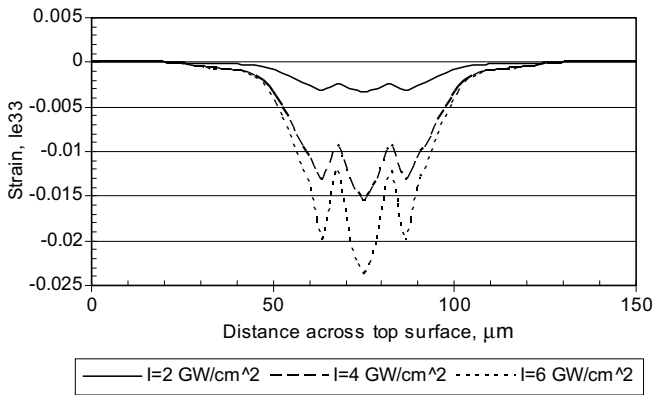

Fig. 7g. Intensity effect on s33.
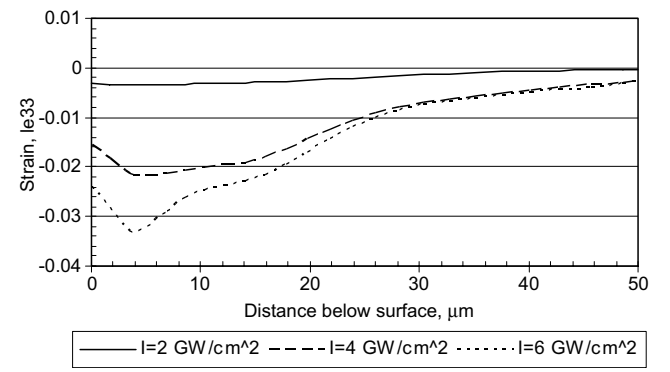

Fig. 7d. Intensity effect on le33.

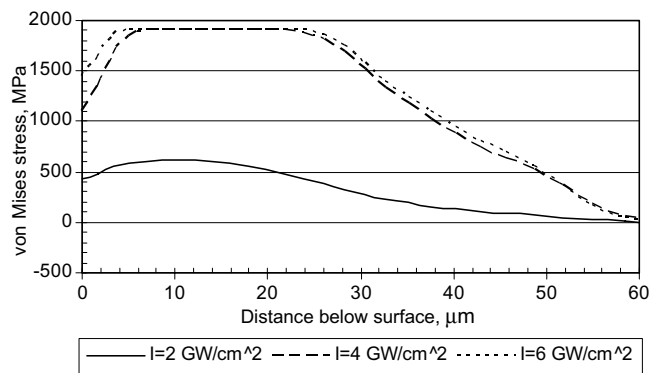Fig. 7h. Intensity effect on le33.

Fig. 7e. Intensity effect on von Mises stress.

maximum defined stress–strain data for the material. Sub-surface stress s11 (Fig. 7f) and s33 (Fig. 7g) are maximum at the surface and decrease with increasing depth.

Strains in subsurface: Fig. 7h shows that the maximum strain occurs at a depth of 3.5 μm for all three laser intensities. The 4 and 6 GW/cm^2 intensities have similarly shaped strain distributions and converge at a depth of ≈30 μm.

4.2.2. Spot size effect

Stresses across top surface: To compare spot size effects, a series of simulations were performed that used a constant laser intensity of 4 GW/cm^2 and spacing equal to the spot

size. For each case only the laser spot radius was varied. Fig. 8a shows the effect of spot size on the von Mises stress distribution across the top surface. The smallest spot size ($R = 3\ \mu m$) gives the most uniform stress distribution but also the smallest peak amplitude. Further increasing the spot size ($R = 6\ \mu m$) serves to increase the peak magnitude but causes a decrease in uniformity. The largest spot size ($R = 9\ \mu m$) slightly increases both the peak stress magnitude and uniformity. Stress component s11 across the top surface is shown in Fig. 8b. The smallest spot size ($R = 3\ \mu m$) provides the most uniformity but also the smallest peak magnitude. The larger spot sizes attain nearly equal maximum peak stress values (-3 GPa) but the largest spot size ($R = 9\ \mu m$) has greater variation across the surface. The stress component associated with the direction of laser propagation, s33, is shown in Fig. 8c. Maximum stress is obtained for the larger spot sizes, $R = 6\ \mu m$ and $R = 9\ \mu m$, but the peak to peak variation is larger for the largest spot size ($R = 9\ \mu m$).

Strains across top surface: Fig. 8d shows the strain le33 variation across the top surface. Increasing the spot size induces larger strains and hence greater deformation at the surface. With the same spacing and laser intensity, a larger spot size also makes more interference of the adjacent peening zones.

Stresses in subsurface: Fig. 8e shows von Mises stress as a function of subsurface depth. All three spot sizes attain a maximum value (1.9 GPa) at a depth of $\approx 4\ \mu m$ but increasing spot size causes an increase in the affected depth. Stress components s11 (Fig. 8f) and s33 (Fig. 8g) are maximum at the surface and decrease with increasing depth. The larger spot sizes attain equal surface stress values but the largest spot size ($R = 9\ \mu m$) has increased magnitudes at depths greater than 2 μm.

Strains in subsurface: Strain variation in the subsurface is shown in Fig. 8h. Near surface strain is nearly equal for spot sizes $R = 3\ \mu m$ and $R = 6\ \mu m$ to a depth of 3 μm. After this depth the larger spot size ($R = 6\ \mu m$) continues to increase in magnitude to a depth of 9 μm. The largest spot size ($R = 9\ \mu m$) achieves the largest surface strain and reaches a maximum at a depth of 4 μm. In the depth range of 6.5–13.5 μm the strain for $R = 6\ \mu m$ is

Fig. 8b. Spot size effect on s11.

Fig. 8c. Spot size effect on s33.

Fig. 8d. Spot size effect on le33.

greater than for $R = 9\ \mu m$. At deeper depths the strain magnitudes decrease with direct relation to spot size.

4.2.3. Spacing effect

Stresses across top surface: The effect of spacing was performed by maintaining constant pressure intensity ($I = 4\ GW/cm^2$) and laser spot size ($R = 6\ \mu m$). The spacing between adjacent laser spots was 6, 12, and 24 μm. von Mises stress distribution across the top surface is shown in Fig. 9a. The closer spacing values ($S = 6\ \mu m$ and
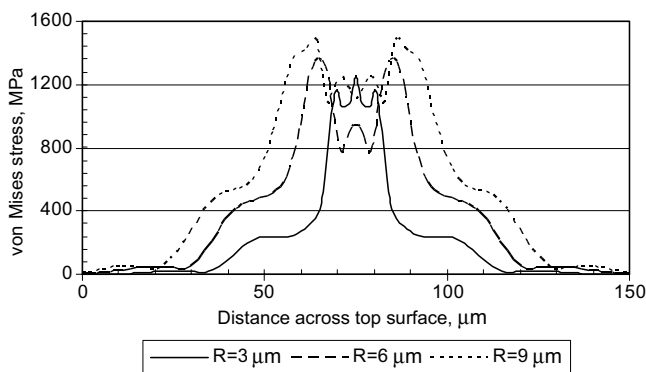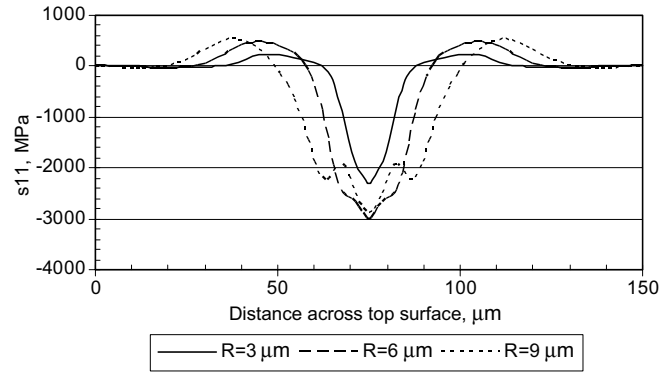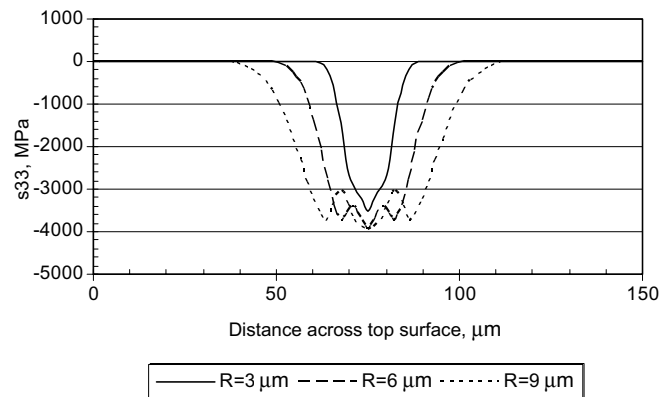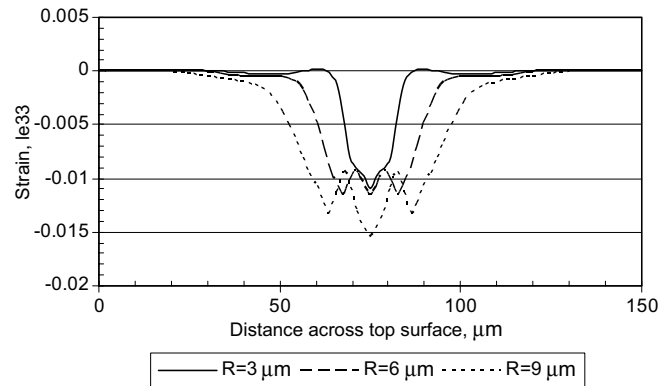

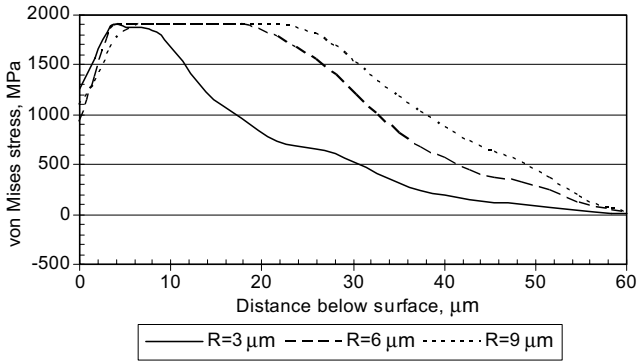Fig. 8a. Spot size effect on von Mises stress.
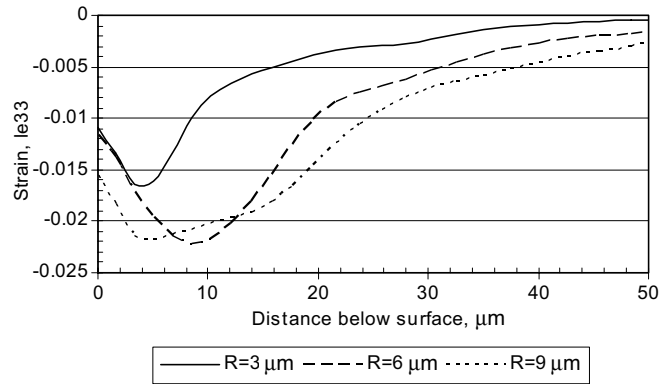
Fig. 8e. Spot size effect on von Mises stress.

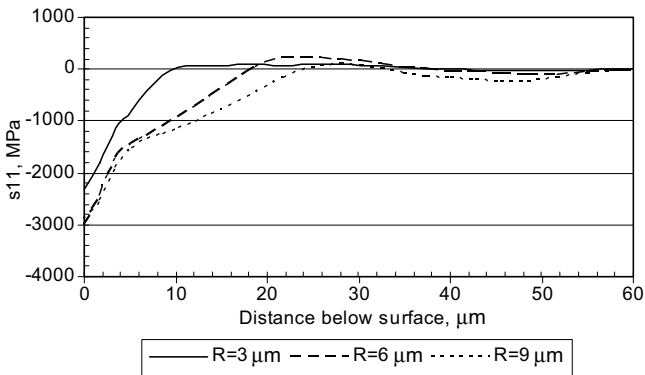Fig. 8h. Spot size effect on le33.
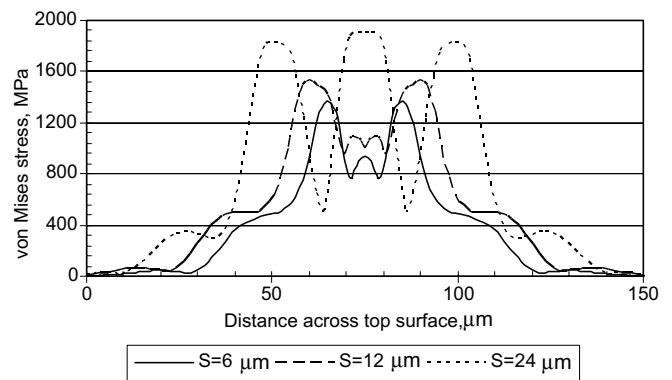

Fig. 8f. Spot size effect on s11.
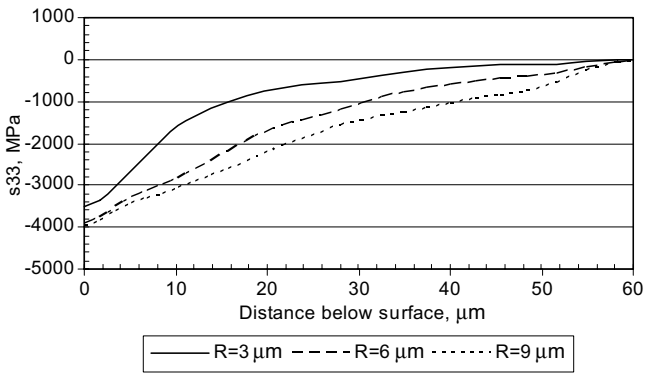

Fig. 9a. Spacing effect on von Mises stress.
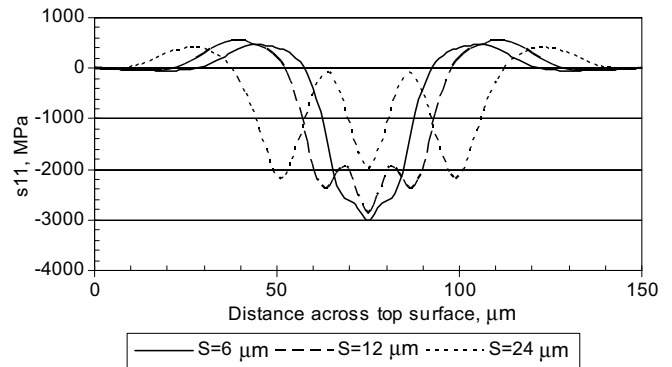

Fig. 8g. Spot size effect on s33.

Fig. 9b. Spacing effect on s11.

$S = 12 \, \mu m$) cause decreased magnitudes of stress at the central spot due to interactions between adjacent shock peened zones. At a spacing of $S = 24 \, \mu m$, the spots do not overlap and a uniform stress pattern is observed at each zone. Increasing the spacing also increases the peak magnitude of stress; however, the peak to peak variation within each case is much larger. Fig. 9b shows that both the magnitude and uniformity of s11 is decreased with increased spacing. Fig. 9c shows that equal peak s33 stress magnitudes are obtained regardless of spacing, but the uniformity of stress is greatly reduced as spacing is increased.

Strains across top surface: Strain le33 across the surface is shown in Fig. 9d. Smaller spacing induces smaller displacement gradients and a more uniform surface profile. Increasing spacing also increases the strain in the central peened zone.

Stresses in subsurface: The von Mises distribution in the subsurface is shown in Fig. 9e. Maximum von Mises stress for the smaller spacing ($S = 6 \, \mu m$ and $S = 12 \, \mu m$) occurs at a depth below the surface due to interactions between adjacent LSP zones. For the $S = 24 \, \mu m$ case, the maximum von Mises stress is located at the surface and begins to decrease at a depth of $7 \, \mu m$. The maximum stress s11 (Fig. 9f) is
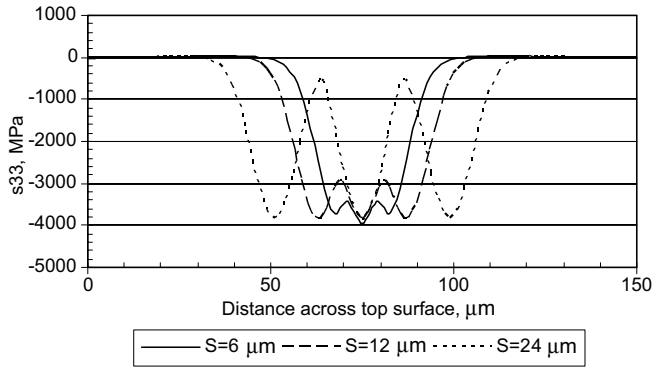
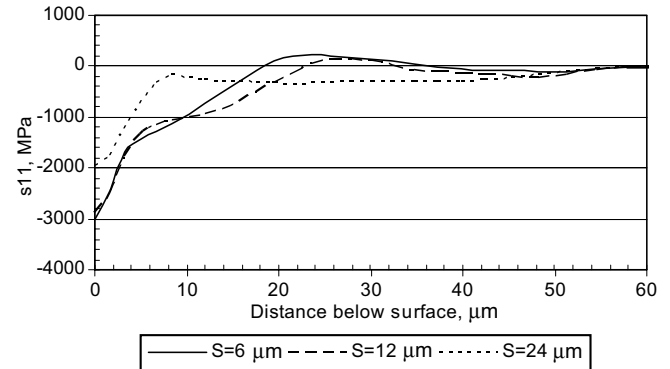Fig. 9c. Spacing effect on s33.
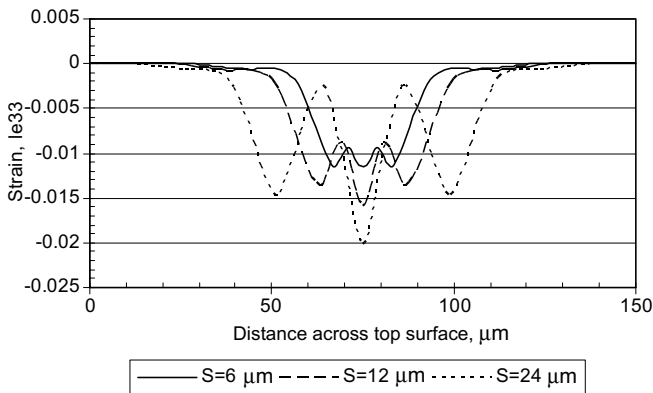

Fig. 9f. Spacing effect on s11.

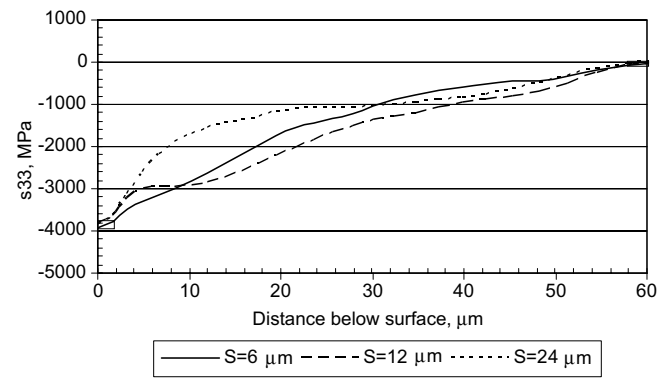Fig. 9d. Spacing effect on le33.

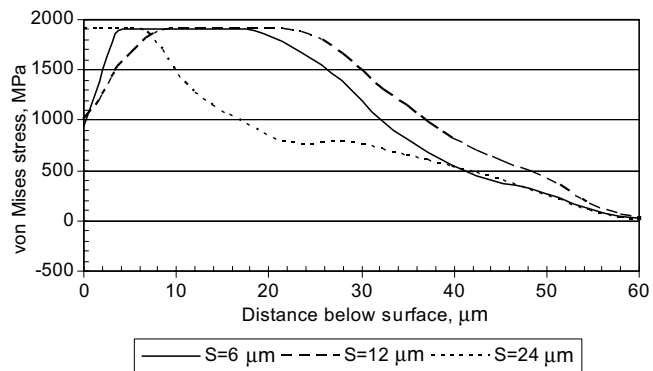Fig. 9g. Spacing effect on s33.
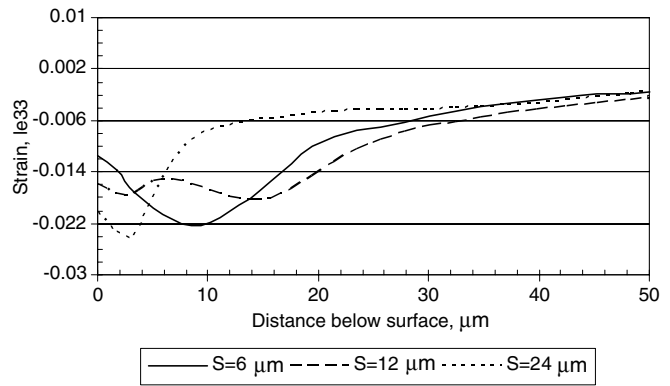

Fig. 9e. Spacing effect on von Mises stress.

Fig. 9h. Spacing effect on le33.

located at the surface for all three cases, but the magnitude is increased for the smaller spacings ($S = 6\,\mu m$ and $S = 12\,\mu m$) due to interaction between the zones. Fig. 9g shows that maximum stress s33 is located at the surface and is equal in magnitude for all cases. Its magnitude decreases more rapidly for the largest spacing ($S = 24\,\mu m$). At depths greater than 9 μm the largest magnitude occurs with a spacing of $S = 12\,\mu m$.

Strains in subsurface: Fig. 9h shows the strain le33 reaches a maximum below the surface for all cases. The greatest magnitude occurs at a depth of 2.2 μm for a spacing of $S = 24\,\mu m$, but rapidly decreases after a depth of

2.5 μm. For the smaller spacings, $S = 6\,\mu m$ and $S = 12\,\mu m$, the strain is much larger at depths greater than 6 μm.

5. Conclusion

FEA simulations of LSP in single and multiple passes were preformed to compare with the measured residual stress data. A DOE based FEA simulations of massive parallel LSP were also performed to determine the effects of laser intensity, laser spot size, and peening spacing on the stress and strain distribution across the top surface and

in the subsurface. The results can be summarized by the following statements:

- A massive parallel LSP simulation with spatial and temporal shock wave pressure has been developed and the simulated residual stresses agree with the measured data in trend, but differ in magnitude. The interactions between adjacent peening zones are significant to the resultant surface integrity.
- Increasing the laser intensity increases both the stress magnitude and affected depth.
- Use of smaller laser spot sizes decreases the largest magnitude of residual stress and also decreases the depth affected by LSP. Larger spot sizes have less energy attenuation and cause more plastic deformation.
- Spacing between peening zones is critical for the uniformity of mechanical properties across the surface. The greatest uniformity and largest stress magnitudes are achieved by overlapping of the laser spots.

Acknowledgement

References

[1] Clauer AH, Ford CT, Ford SC. The effects of laser shock processing on the fatigue properties of T-3 aluminum. In: Lasers in materials processing. Metals Park (OH): American Society of Metals; 1983. p. 7–22.

[2] Clauer AH, Koucky JR. Laser shock processing increases the fatigue life of metal parts. J Mater Process Technol 1991;6:3–5.

[3] Peyre P, Fabbro R, Merrien P, Lieurade HP. Laser shock processing of aluminum alloys. Application to high cycle fatigue behavior. Mater Sci Eng A 1996;210:102–13.

[4] Vaccari JA. Laser shocking extends fatigue life. Amer. Mach. 1992:62–4.

[5] Ashley S. Powerful laser means better peening. Mech Eng 1998;120:12.

[6] Brown AS. A shocking way to strengthen metal. Aerospace Am 1998:21–3.

[7] Banas G, Elsayed-Ali HE, Lawrence FV, Rigsbee JM. Laser shock-induced mechanical and microstructural modification of welded maraging steel. J Appl Phys 1990;67:2380–4.

[8] Clauer AH, Holbrook JH, Fairand BP. Effects of laser induced shock waves on metals. In: Meyers MA, Murr LE, editors. Shock waves and high-strain-rate phenomena in metals. New York: Plenum Publishing Corporation; 1981. p. 675–702.

[9] Yakimets I, Richard C, Béranger G, Peyre P. Laser peening processing effect on mechanical and tribological properties of rolling steel 100Cr6. Wear 2004;256(3–4):311–20.

[10] Nalla RK, Altenberger I, Noster U, Liu GY, Scholtes B, Ritchie RO. On the influence of mechanical surface treatments – deep rolling and laser shock peening – on the fatigue behavior of Ti–6Al–4V at ambient and elevated temperatures. Mater Sci Eng A 2003;355:216–30.

[11] Nikitin I, Sholtes B, Maier HJ, Altenberger I. High temperature fatigue behavior and residual stress stability of laser-shock peened and deep rolled austenitic steel AISI 304. Scripta Mater 2004;50:1345–50.

[12] Montross CS, Wei T, Ye L, Clark G, Mai YW. Laser shock peening and it's effects on microstructure and properties of metal alloys: a review. Int J Fatigue 2002;24:1021–36.

[13] Fabbro R, Peyre P, Berthe L, Sherpereel X. Physics and application of laser – shock processing. J Laser Appl 1998;10:265–79.

[14] Peyre P, Berthe L, Scherpereel X, Fabbro R. Laser-shock processing of aluminum coated 55C1 steel in water-confinement regime, characterization and application to high-cycle fatigue behavior. J Mater Sci 1998;33:1421–9.

[15] Ruschau JJ, John R, Thompson SR, Nicholas T. Fatigue crack nucleation and growth rate behavior of laser shock peened titanium. Int J Fatigue 1999;21:S199–209.

[16] Zhang W, Yao YL, Noyan IC. Microscale laser shock peening of thin films, Part 1: experiment modeling and simulation. J Manuf Sci Eng 2004;126:10–7.

[17] Clauer AH, Holbrock JH. Effects of laser induced shock waves on metals. Shock waves and high strain phenomena in metals – concepts and applications. New York: Plenum; 1981. p. 675–702.

[18] Fabbro R, Fournier J, Ballard P, Devaux D, Virmont J. Physical study of laser-produced plasma in confined geometry. J Appl Phys 1990;68(2):775–84.

[19] Braisted W, Brockman R. Finite element simulation of laser shock peening. Int J Fatigue 1999;21:719–24.

[20] Ding K, Ye L. Three-dimensional dynamic finite element analysis of multiple laser shock peening process. Surf Eng 2003;19:351–8.

[21] Zhang W, Yao YL. Micro scale laser shock processing of metallic components. J Manuf Sci Eng 2002;124:369–78.

[22] ABAQUS, Inc., ABAQUS User's Manual, Ver. 6.4, Pawtucket, RI, 2003.